

Trends in the Frozen Ground Temperature on the Tibetan Plateau Simulated by RegCM4.7-CLM4.5

Jiangxin Luo¹, Shihua Lyu¹, Xuewei Fang¹, and Yigang Liu¹

¹Chengdu University of Information Technology

November 21, 2022

Abstract

The changing characteristics of the frozen ground (FG) are essential indicators of climate change. The soil temperature (ST) on the Tibetan Plateau (TP) during 1987- 2018 was simulated using the coupled model of RegCM4.7-CLM4.5. The results show that there is a significant warming trend in the ST on the TP, and the warming trend is higher in October-May ($0.040 [?] \text{decade}^{-1}$) than in June-September ($0.026 [?] \text{decade}^{-1}$), with the maximum value in February ($0.058 [?] \text{decade}^{-1}$). Spatially, the warming is most significant in the Three River Source Region ($0.15 \sim 0.20 [?] \text{decade}^{-1}$) and near the Himalayas and Kunlun Mountains ($0.20 \sim 0.25 [?] \text{decade}^{-1}$), with the warming trend greater in winter and spring than in summer and autumn. Air temperature (AT), total precipitation (TPR), maximum snow depth (MSD), and maximum frozen ground depth (MFD) can significantly affect the ST variation. The AT ($R=0.851$) and TPR ($R=0.411$) can accelerate the soil warming, while the MSD ($R=-0.381$) and the MFD ($R=-0.770$) can decelerate the soil warming. The AT has a strong influence on the ST in all four seasons, while the effect of the TPR is strongest in autumn ($R=0.836$). The retarding effects of the MSD and the MFD are strongest in summer ($R=-0.772$ and -0.35 respectively). Both the observation data and numerical simulation analyses indicate that the FG on the TP shows a degradation trend, and the consequent hydrological, ecological, and climatic effects deserve sufficient attention.

Trends in the Frozen Ground Temperature on the Tibetan Plateau Simulated by RegCM4.7-CLM4.5

Jiangxin Luo¹, Shihua Lyu^{1,2}, Xuewei Fang¹ and Yigang Liu¹

Abstract: The changing characteristics of the frozen ground (FG) are essential indicators of climate change. The soil temperature (ST) on the Tibetan Plateau (TP) during 1987- 2018 was simulated using the coupled model of RegCM4.7-CLM4.5. The results show that there is a significant warming trend in the ST on the TP, and the warming trend is higher in October-May ($0.040\text{ }^{\circ}\text{C}\cdot\text{decade}^{-1}$) than in June-September ($0.026\text{ }^{\circ}\text{C}\cdot\text{decade}^{-1}$), with the maximum value in February ($0.058\text{ }^{\circ}\text{C}\cdot\text{decade}^{-1}$). Spatially, the warming is most significant in the Three River Source Region ($0.15\sim 0.20\text{ }^{\circ}\text{C}\cdot\text{decade}^{-1}$) and near the Himalayas and Kunlun Mountains ($0.20\sim 25\text{ }^{\circ}\text{C}\cdot\text{decade}^{-1}$), with the warming trend greater in winter and spring than in summer and autumn. Air temperature (AT), total precipitation (TPR), maximum snow depth (MSD), and maximum frozen ground depth (MFD) can significantly affect the ST variation. The AT ($R=0.851$) and TPR ($R=0.411$) can accelerate the soil warming, while the MSD ($R=-0.381$) and the MFD ($R=-0.770$) can decelerate the soil warming. The AT has a strong influence on the ST in all the four seasons, while the effect of the TPR is strongest in autumn ($R=0.836$). The retarding effects of the MSD and the MFD are strongest in summer ($R=-0.772$ and -0.35 respectively). Both the observation data and numerical simulation analyses indicate that the FG on the TP shows a degradation trend, and the consequent hydrological, ecological, and climatic effects deserve sufficient attention.

1. Introduction

Frozen ground (FG) refers to all kinds of rocks and soils that are below 0°C and contain ice. According to the freezing time length, FG is divided into two categories: seasonally frozen ground (SFG) and permafrost. Permafrost is defined as an area covered by perennially frozen soil where the deep soil temperature (ST) remains at or below 0°C for two or more consecutive years. Permafrost is mainly found in colder regions at high latitudes and high altitudes where the average annual air temperature (AAT) is below 0°C . The soil partially melts near the surface in summer and refreezes in winter until the entire soil column is completely frozen. SFG is distributed in areas where the AAT is higher than 0°C . The soil freezes in winter, starts to melt in spring and thaws completely in summer (Gao 2017). The FG acts as a buffer for the land-air interaction, which releases and absorbs soil heat capacity slowly and may have a lasting effect on atmospheric circulations (Wang et al. 2001, Mackay 2008).

The Tibetan Plateau (TP) is known as the “third pole of the world” and the “water tower of Asia”. Due to the widely distributed permafrost and SFG, and its

¹Chengdu University of Information Technology, Chengdu, China.

²Collaborative Innovation Center on Forecast and Evaluation of Meteorological Disasters, Nanjing University of Information Science and Technology, Nanjing, China.

Corresponding author: S. H. Lyu, School of Atmospheric Sciences, Chengdu University of Information Technology (CUIT), Chengdu 610225, China. (slu@cuit.edu.cn)

unique geographic location and altitude, it greatly influences the climate characteristics of China and Asia. The FG area on the TP accounts for 70% of the total FG area in China, and the total FG area accounts for 22.3% of the total land area (Zhou et al. 1982). The hydrothermal changes caused by seasonal freeze-thaw processes on the TP is an important exogenous source of the climate change in East Asia, and the maximum frozen ground depth (MFD) on the TP can serve as a signal for the summer precipitation in China (Wang et al. 2003, Zhang et al. 2004, Zhao and Moore 2004).

The soil heat fluxes are generally positive in most FG areas on the TP, resulting in the permafrost in a degradation process, and it is difficult to capture these changes in reanalysis data (Chen et al. 2006, Yang et al. 2014). Changes in the freeze-thaw cycle of the near-surface soils have significant impacts on the hydrological processes, ecosystems, and engineering operations on the TP. Changes in the permafrost thickness are negatively correlated with the ecological carrying capacity of grasslands, with one unit of increase in the former corresponding to 0.1 unit of decrease in the latter (Fang and Zhu 2019). With the melting of FG, more carbon may be emitted into the atmosphere in the future, and the sequestration capacity of vegetation ecosystems will be reduced. The analysis of the causes of FG changes shows that the increase in annual minimum and winter air temperature (AT) leads to earlier thawing and later freezing of FG, as well as longer duration of thawing, and shorter duration of freezing. The most significant changes occur in the northeast and the southwest of the TP (Wang et al. 2017, Li et al. 2012). Global warming will lead to more severe FG degradation. Statistical analysis of the FG at the observation stations along the Qinghai-Tibet Railway (QTR) shows that the thickness of the active layer increases at an average rate of $7.5\text{cm}\cdot\text{year}^{-1}$ from 1995 to 2007, which is mainly caused by the increase in summer AT, while the changes in winter AT and snow cover have less effect (Wu et al. 2010). Numerical experiments show that the permafrost at altitudes of 3500~3900 m on the TP decreases by about 500km^2 from 1971 to 2013, with a decrease rate of $3.2\text{ cm}\cdot\text{decade}^{-1}$ for the maximum freezing depth of SFG and an increase rate of $4.3\text{ cm}\cdot\text{decade}^{-1}$ for the active layer thickness in the permafrost zone (Gao et al. 2018). The study of the FG on the TP, the critical water-supply area for the Yellow River, the Yangtze River and the Lancang River, is directly related to the protection of water resources and ecosystems in China, as well as to climate prediction in Asia.

ST is an important indicator of FG change, and the definitions of freezing and thawing processes, freezing depth and active layer thickness in the existing studies are based on ST (Cuo et al. 2015, Gao et al. 2018, Guo et al. 2011). In this paper, a coupled numerical model was utilized to simulate the TP land surface processes for 32 years and the climate change characteristics of the FG and the ST are discussed. In addition, the meteorological factors influencing the FG changes are analyzed, which can provide a scientific basis for the climate prediction in Asia and the protection of water resources and ecological environment in China.

2. Experimental design

The unfrozen water scheme designed in the Community Land Model version 4.5 (CLM4.5) enables the model to simulate the liquid water remaining in the soil when the soil freezes in winter, and to effectively simulate the hydrothermal changes in the soil during freeze-thaw periods (Li et al. 2018, Xie et al. 2017). The Regional Climate Model (RegCM) can capture the weather processes caused by small-scale perturbations and has a good ability to simulate the summer precipitation in eastern China and the spatial distribution of the FG on the TP (Gao et al. 2008, Li 2013, Yu 2011, Kong et al. 2019, Zhou 2007). The CLM4.5 has been coupled into the RegCM4.7, and users can enable the CLM4.5 module when installing the RegCM4.7 for a better analysis of land-air interactions. Luo et al. (2020) have verified that the RegCM4.7-CLM4.5 has an excellent capability to simulate the hydrothermal changes of FG during freeze-thaw periods on the TP.

By using the RegCM4.7 and the land surface component in the CLM4.5, we performed a numerical simulation on the TP and its surroundings, as shown in Figure 1. The simulation period was set from January 1, 1982 to December 31, 2018, with the first 5 years as the spin-up and the following 32 years (January 1, 1987 to December 31, 2018) for the analysis. The model configuration is determined after several sensitivity tests. The Lambert projection is applied, with the center point at 33°N, 87°E, and the simulation grids of 80 (meridional) \times 120 (zonal). The number of vertical layers is 18, with the top pressure of 50 hPa and the horizontal resolution of 30km. The time integration step is 60 seconds. The European Centre for Medium-Range Weather Forecasts (ECMWF) Interim Re-Analysis data, with the horizontal resolution of 1.5° \times 1.5° (EIN15), is utilized as the initial field, and the weekly optimum interpolation (OI_WK) sea surface temperature (SST) is applied. The land surface module outputs data 24-hourly. The other parameterization schemes are listed in Table 1.

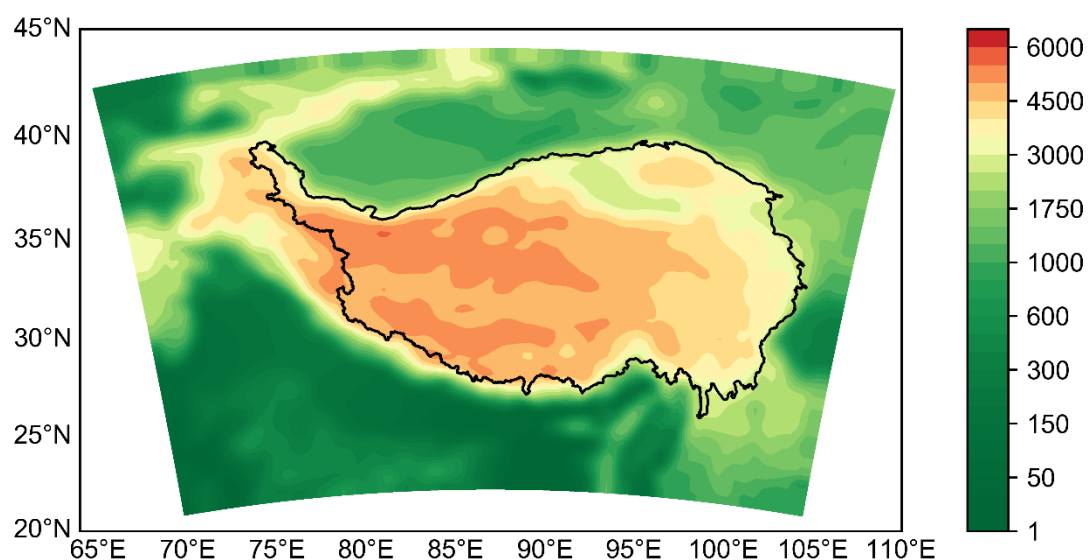


Figure 1. The geographical location and the terrain height (unit: m) of the analysis region.

The black curve outlines the Tibetan Plateau.

Table 1. Selection of parameterization schemes.

Physics	Scheme
---------	--------

Lateral Boundary conditions scheme	Relaxation, linear technique
Boundary layer scheme	Holsting PBL (Holtslag, 1990)
Cumulus convection scheme overland	Emanuel (1991)
Large-scale precipitation	SUBEX (Beheng, 1994; Giorgi, 1990)
Ocean flux scheme	Zeng (1998)
IPCC scenario	A1B

Furthermore, two non-parametric methods, the Modified Mann-Kendall trend (MMK) test (Mann 1945, Kendall 1955, Hamed & Rao 1998) and Sen's slope estimator (Sen 1968) were used to analyze the trends in the ST and other meteorological variables on the monthly, seasonal and annual scales based on the daily data from the CLM4.5. The four seasons of spring (March, April, and May), summer (June, July, and August), autumn (September, October, and November), and winter (December, January, and February) were defined. These two methods have both been widely validated in practical applications (Fang et al. 2019, Luo et al. 2016). In cases with the sample size n greater than 10, the standard normal test statistic Z for the MMK is computed with Eq. (1-3):

$$Z = \begin{cases} \frac{S-1}{\sqrt{Var^*(S)}}, & \text{if } S > 0 \\ 0, & \text{if } S = 0 \\ \frac{S+1}{\sqrt{Var^*(S)}}, & \text{if } S < 0 \end{cases} \quad (1)$$

$$S = \sum_{i=1}^{n-1} \sum_{j=i+1}^n sgn(x_j - x_i) \quad (2)$$

$$sgn(x_j - x_i) = \begin{cases} +1, & \text{if } x_j - x_i > 0 \\ 0, & \text{if } x_j - x_i = 0 \\ -1, & \text{if } x_j - x_i < 0 \end{cases} \quad (3)$$

Where S represents the sum of the deviation characteristics between the values at two moments i and j ($j > i$) in a single time series. The autocorrelation effective values have been removed from the time series. The significance test for the trend is done at a specific significance level. If $|Z| > Z_{1-\alpha}$, the null hypothesis is rejected and there is a significant trend in the time series. In Eq. (1), positive values of Z indicate increasing trends of the time series while negative values indicate decreasing trends.

The Sen's slope estimator is used to estimate the median slope Q_{med} for a time series, computed as Eq. (4-5):

$$Q_{med} = \begin{cases} Q_{[(N+1)/2]}, & \text{if } N \text{ is odd} \\ \frac{Q_{[N/2]} + Q_{[(N+2)/2]}}{2}, & \text{if } N \text{ is even} \end{cases} \quad (4)$$

$$Q_i = \frac{x_j - x_k}{j - k} \quad \text{for } i = 1, \dots, N \quad (5)$$

Where x_j and x_k denote data values at time j and k ($j > k$), respectively. The detailed computational procedures for Z and Q , as well as the significance test for Q_{med} , can be found in Luo et al. (2016).

3. Results

3.1 Soil temperature climatology

In CLM4.5, the soil column is divided into 15 layers, with the soil depths of 0.7 cm, 2.8 cm, 6.2 cm, 11.9 cm, 21.2 cm, 36.6 cm, 62.0 cm, 103.8 cm, 172.8 cm, 286.5 cm, 473.9 cm, 783.0 cm, 1293.5 cm, 2132.7 cm and 3517.8 cm, respectively. In this paper, we chose the soil depths of 0.7~286.5 cm for analysis. After the ST on the TP was extracted from the boundary file, the monthly averages from 1987-2018 were calculated and plotted as a line graph in Figure 2. The STs in the 0.7~21.2 cm layers reach the maximum values of 18.486 °C, 18.394 °C, 18.240 °C, 17.962 °C and 17.459 °C in July and the minimum values of -2.205 °C, -2.091 °C, -1.933 °C, -1.703 °C and -1.320 °C in January. However, the STs in the 36.6~103.8 cm layers demonstrate the peak values of 16.654 °C, 15.695 °C and 13.991 °C in August. The minimum STs at 36.6 cm and 62.0 cm appear in January, with the values of -0.639 °C and 0.562 °C, and that at 103.8 cm appears in February (2.072 °C). In the layers of 172.8 cm and 286.5 cm, the STs maximize in September (11.786 °C) and October (9.368 °C), respectively, and minimize in February (3.773 °C) and March (5.193 °C), respectively.

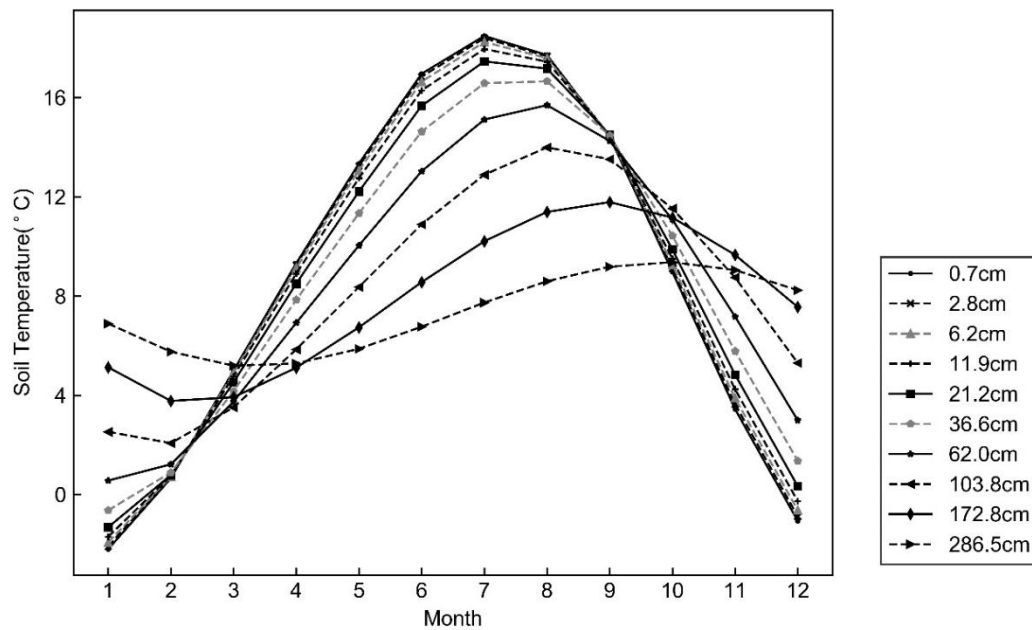


Figure 2. Monthly variations of the average soil temperature on the TP.

The ST is periodically influenced by the AT, with a certain lag in both warming and cooling as the soil depth increases. It makes the deep ST higher than the shallow ST in the cold seasons (December to February) and lower in the warm seasons (June to August).

3.2 Soil temperature trends

The trends in the monthly mean STs on the TP at 0.7~286.5 cm during 1987-2018 are shown in Table 2~3. The ST increases at all the layers in each month, and both Z and Q are consistently positive. The trends are greatest in February, with an average of $0.058\text{ }^{\circ}\text{C}\cdot\text{decade}^{-1}$, and lowest in September, with an average of $0.024\text{ }^{\circ}\text{C}\cdot\text{decade}^{-1}$. The increase in the ST is greater in the cold seasons (October-May), averaged above $0.03\text{ }^{\circ}\text{C}\cdot\text{decade}^{-1}$, while relatively smaller in the

168 warm seasons (June-September), with the trend of 0.019~0.037 °C·decade⁻¹. However,
 169 the soil warming trends are more statistically significant in the relatively warm
 170 seasons, with the trends in all the layers passing the 0.01 significance test in
 171 March-August. On the contrary, the warming trends in the 0.7~36.6 cm layers failed
 172 the 0.05 significance test in December-January, and the failure is common in
 173 November and February in the shallow and middle layers.

174 **Table 2.** Modified Mann-Kendall test statistic (Z) for the monthly mean soil temperature
 175 (°C·decade⁻¹) during 1987-2018. Significance levels: * $\alpha=0.05$, ** $\alpha=0.01$.

Month	0.7cm	2.8cm	6.2cm	11.9cm	21.2cm	36.6cm	62.0cm	103.8cm	172.8cm	286.5cm
Jan	0.341	0.470	0.470	1.171	0.632	1.461	1.897	5.052**	5.433**	12.758**
Feb	2.105*	1.346	1.476	1.638	3.564**	1.897	2.027*	3.227**	8.453**	12.735**
Mar	3.616**	3.714**	3.746**	3.876**	3.973**	4.038**	4.168**	4.622**	5.303**	6.860**
Apr	3.292**	3.357**	3.454**	5.649**	3.908**	5.969**	8.090**	5.076**	7.799**	5.652**
May	2.903**	3.448**	3.033**	4.286**	4.711**	4.330**	6.544**	5.660**	6.114**	6.827**
Jun	8.492**	6.738**	5.619**	3.195**	6.116**	4.135**	4.654**	11.643**	16.270**	9.861**
Jul	2.514**	2.546**	2.708**	3.000**	3.389**	3.746**	4.417**	8.946**	10.438**	13.448**
Aug	3.616**	3.681**	4.985**	5.523**	4.265**	5.640**	6.602**	6.049**	6.892**	7.443**
Sep	1.800	2.273*	1.768	3.201**	2.157*	3.860**	4.883**	5.887**	9.395**	7.541**
Oct	2.611**	2.676**	2.708**	2.708**	2.870**	2.903**	3.941**	5.206**	6.827**	7.703**
Nov	1.957	3.287**	1.800	2.011*	1.995*	2.449*	3.519**	5.043**	6.503**	7.541**
Dec	0.025	0.016	0.380	0.470	0.762	1.541	2.935**	8.781**	6.114**	9.358**

176 In terms of vertical soil stratification, the ST warming trends decrease with the
 177 increasing soil depth. However, the ST trends of deep soil are more significant than
 178 those in the shallow and middle layers in December-February. Besides, the
 179 inter-monthly ST variation of the deep soil also lags slightly behind those in the
 180 shallow and middle layers. The warming trends in the 0.7~36.6 cm soil layers are
 181 smaller in August than in September, and the trends in the 62.0~286.5 cm layers are
 182 higher in August than in September. This is related to the fact that the ST transfer
 183 from shallow to deep layers requires a certain time. The effects of other
 184 meteorological factors on the ST warming trends will be discussed in section 3.3.

185 **Table 3.** Same as Table 2, but for the Sen's slope estimator (Q).

Month	0.7cm	2.8cm	6.2cm	11.9cm	21.2cm	36.6cm	62.0cm	103.8cm	172.8cm	286.5cm
Jan	0.063	0.062	0.060	0.058	0.054	0.047	0.040	0.030**	0.023**	0.016**
Feb	0.075*	0.076	0.075	0.072	0.067**	0.060	0.053*	0.044**	0.031**	0.021**
Mar	0.052**	0.052**	0.051**	0.050**	0.048**	0.046**	0.041**	0.036**	0.028**	0.022**
Apr	0.048**	0.048**	0.047**	0.045**	0.044**	0.041**	0.037**	0.031**	0.024**	0.021**
May	0.043**	0.042**	0.041**	0.039**	0.037**	0.033**	0.029**	0.025**	0.024**	0.022**
Jun	0.037**	0.036**	0.036**	0.034**	0.032**	0.029**	0.025**	0.022**	0.020**	0.021**

Jul	0.031 ^{**}	0.031 ^{**}	0.030 ^{**}	0.030 ^{**}	0.029 ^{**}	0.028 ^{**}	0.027 ^{**}	0.024 ^{**}	0.020 ^{**}	0.020 ^{**}
Aug	0.029 ^{**}	0.028 ^{**}	0.028 ^{**}	0.027 ^{**}	0.026 ^{**}	0.024 ^{**}	0.023 ^{**}	0.021 ^{**}	0.020 ^{**}	0.019 ^{**}
Sep	0.031	0.030 [*]	0.030	0.029 ^{**}	0.027 [*]	0.025 ^{**}	0.020 ^{**}	0.016 ^{**}	0.016 ^{**}	0.019 ^{**}
Oct	0.042 ^{**}	0.041 ^{**}	0.040 ^{**}	0.038 ^{**}	0.036 ^{**}	0.032 ^{**}	0.026 ^{**}	0.018 ^{**}	0.014 ^{**}	0.017 ^{**}
Nov	0.046	0.044 ^{**}	0.043	0.041 [*]	0.039 [*]	0.035 [*]	0.028 ^{**}	0.021 ^{**}	0.015 ^{**}	0.017 ^{**}
Dec	0.052	0.052	0.050	0.049	0.047	0.043	0.036 ^{**}	0.027 ^{**}	0.014 ^{**}	0.017 ^{**}

186 The annual or seasonal trends were calculated by averaging the STs in the
187 shallow (0.7 cm), middle (2.8~21.2 cm) and deep (36.6~286.5 cm) layers separately.
188 Regional shaded maps were also created. For the shallow soil layers (Figure 3), both
189 the seasonal and annual mean STs increased significantly with the trends generally
190 passing the 0.05 significance test. The increasing trends are mainly in the 30°N~35°N
191 region, with the annual trends of 0.05~0.10 °C·decade⁻¹. Among the four seasons, the
192 increasing trends in winter and spring are relatively large, especially in the Three
193 River Source Region (TRSR) (0.15~0.20 °C·decade⁻¹) and over the Himalayas and
194 Kunlun Mountains (0.20~0.25 °C·decade⁻¹). In summer, the large increasing trends
195 are mainly found in the western permafrost region (0.10~0.20 °C·decade⁻¹). In
196 autumn, the increasing trends are distributed near the Himalayas
197 (0.10~0.15 °C·decade⁻¹) and the Kunlun Mountains (0.10~0.20 °C·decade⁻¹), with the
198 trends in fewer areas passing the significance test.

199 For the middle soil layers (Figure 4), the spatial distribution of the warming trend
200 is almost similar to that of the shallow layers, but the annual and seasonal warming
201 trends are about 0.05 °C·decade⁻¹ lower than that of the shallow layers. In winter, the
202 warming trends are still greatest in the TRSR and over the southern Himalayas. As the
203 soil layer deepens (Figure 5), the soil warming trend decreases by another
204 0.05 °C·decade⁻¹, and the trend over the whole TP passes the 0.05 significance test. In
205 winter and spring, the warming trends are still significant in the TRSR and near the
206 Himalayas and Kunlun Mountains.

207 By analyzing the STs at nine observation stations in the TRSR from 1980 to
208 2014, Luo et al. (2016) found that the STs at all the nine stations show significant
209 warming trends, with an average of 0.533 °C·decade⁻¹, and all the trends pass the 0.01
210 significance test. The maximum warming of the surface (0 cm) soil layer occurs in
211 winter, while that in the shallow (5 cm, 10 cm, 15 cm and 20 cm) and deep (40 cm, 80
212 cm, 160 cm and 320 cm) layers occurs in summer. Besides, the month with the
213 maximum warming differs significantly among sites and soil layers. Fang et al. (2019)
214 analyzed the STs at 50 sites on the east-central TP from 1960 to 2014 and found that
215 the greatest warming in the surface layer, the shallow layer and the deep layer on the
216 TP occurs in winter (January, about 0.67°C·decade⁻¹), spring (April, about
217 0.49°C·decade⁻¹) and summer (June, about 0.58 °C·decade⁻¹), respectively. The ST
218 warming trends at all the layers analyzed in this paper are consistent on annual,
219 seasonal and monthly scales, and the month with the maximum warming does not
220 show a certain lag with the increasing soil depth. Moreover, the trend values are
221 smaller than those in Fang et al. (2019) and Luo et al. (2016), which may need to be

222 further verified with multiple numerical experiments.

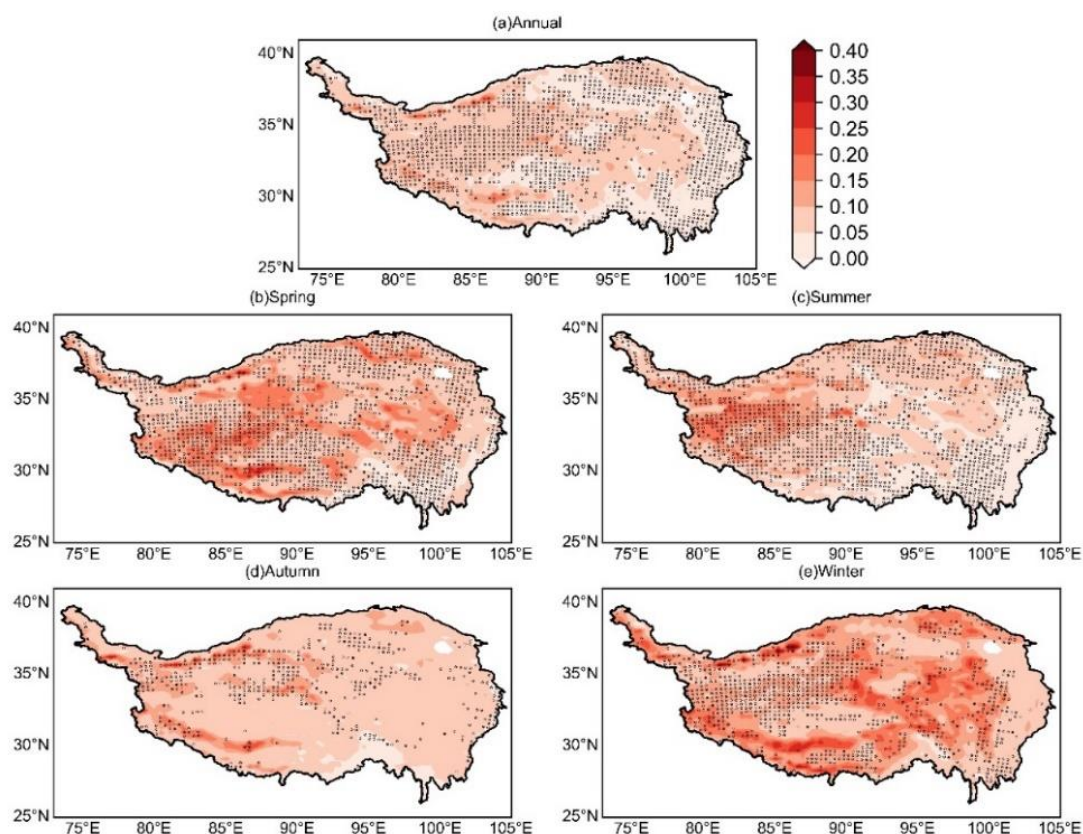


Figure 3. Trends in seasonal and annual mean soil temperature (°C·decade⁻¹) in the shallow layer (0.7 cm). Dotted areas indicate the trends passing the 0.05 significance test.

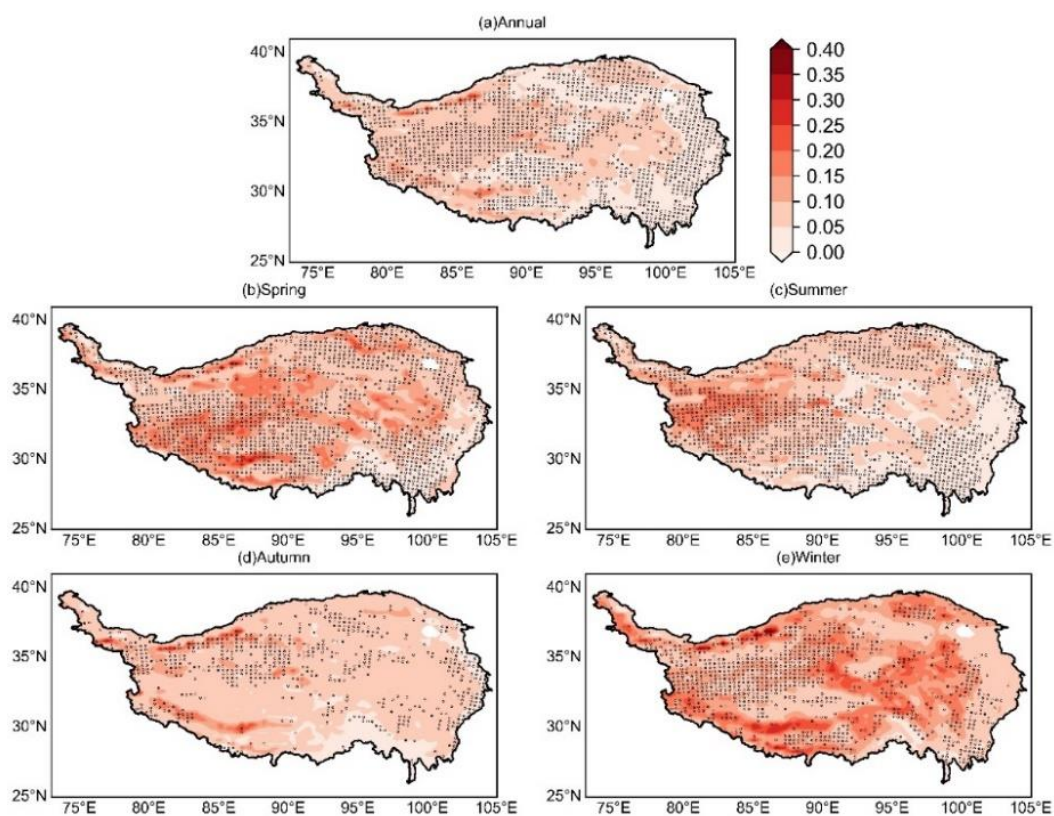


Figure 4. Same as Figure 3, but for the middle layers (2.8 cm, 6.2 cm, 11.9 cm and 21.2 cm)

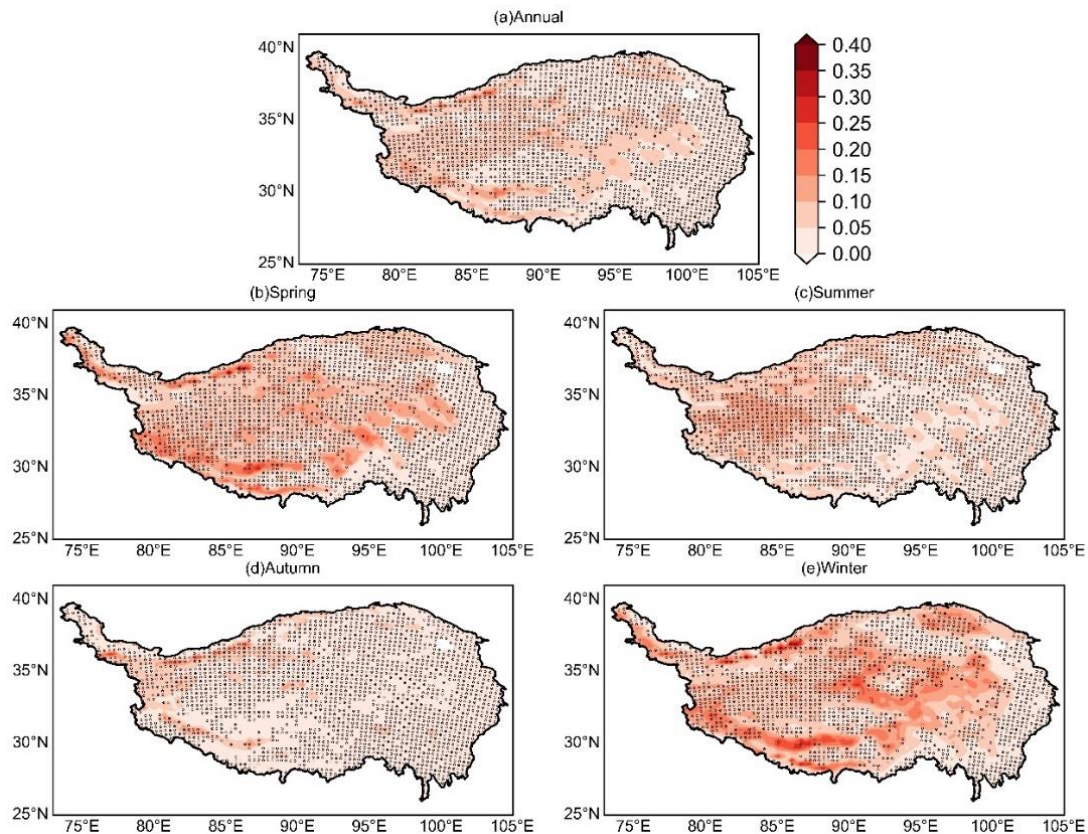


Figure 5. Same as Figure 3, but for the deep layers (36.6 cm, 62.0 cm, 103.8 cm, 172.8 cm and 286.5 cm)

3.3 Relationship between soil temperature and other climate characteristics

The depth where the 0°C isotherm is located in the soil layer is defined as the frozen depth (Wu et al. 2010). The relationships between the ST and the AT, the total precipitation (TPR), the maximum snow depth (MSD) and the maximum frozen ground depth (MFD) are shown in Table 4. The ST is significantly correlated with the AT, with the correlation coefficients (R) averaged above 0.85 and generally passing the 0.01 significance test. The influence of the AT on the ST is most significant in spring, with an average R of 0.928, which is followed by autumn, summer and winter, with the average R of 0.892, 0.857 and 0.560, respectively. Additionally, the correlation decreases with the increasing soil depth. The R between the ST and the AT in the shallow and middle layers generally reaches 0.99 and above in spring, summer and autumn, and the R in winter is lowest, with an average of 0.90. Due to the lagging effect of temperature transfer from shallow to deep soil layers, the STs at 103.8 cm, 172.8 cm, and 286.5 cm reach the highest value in August, September and October, respectively. As a result, the R between the ST at 103.8 cm and the AT is only 0.082, and the correlations at 172.8 cm and 286.5 cm are even negative.

Table 4. Correlation coefficients between the soil temperature and the seasonal and annual air temperature, the total precipitation, the maximum snow depth and the maximum frozen ground

	0.7 cm	2.8 cm	6.2 cm	11.9 cm	21.2 cm	36.6 cm	62.0 cm	103.8 cm	172.8 cm	286.5 cm
Spring										
AT	0.998**	0.998**	0.998**	0.998**	0.997**	0.995**	0.991**	0.978**	0.912**	0.419**
TPR	0.866**	0.867**	0.867**	0.868**	0.870**	0.873**	0.877**	0.879**	0.846**	0.427**
MSD	0.161	0.160	0.159	0.158	0.155	0.150	0.139	0.114	0.026	-0.256
MFD	-0.133	-0.135	-0.138	-0.146	-0.158	-0.176	-0.205*	-0.265**	-0.447**	-0.905**
Summer										
AT	0.987**	0.991**	0.993**	0.989**	0.963**	0.901**	0.806**	0.707**	0.653**	0.581**
TPR	0.646**	0.651**	0.656**	0.659**	0.650**	0.615**	0.556**	0.489**	0.446**	0.379**
MSD	-0.576**	-0.606**	-0.651**	-0.718**	-0.802**	-0.881**	-0.928**	-0.935**	-0.897**	-0.730**
MFD	-0.289**	-0.286**	-0.288**	-0.295**	-0.299**	-0.294**	-0.284**	-0.312**	-0.442**	-0.715**
Autumn										
AT	0.998**	0.998**	0.998**	0.998**	0.998**	0.997**	0.995**	0.983**	0.858**	0.100
TPR	0.950**	0.949**	0.949**	0.948**	0.945**	0.942**	0.935**	0.915**	0.770**	0.055
MSD	-0.833**	-0.834**	-0.834**	-0.833**	-0.832**	-0.830**	-0.826**	-0.815**	-0.703**	-0.085
MFD	-0.037	-0.038	-0.039	-0.040	-0.043	-0.052	-0.080	-0.166	-0.484**	-0.973**
Winter										
AT	0.911**	0.918**	0.924**	0.928**	0.909**	0.785**	0.443**	0.082	-0.131	-0.174
TPR	0.461**	0.441**	0.411**	0.358**	0.248*	0.016	-0.315**	-0.537**	-0.628**	-0.600**
MSD	0.465**	0.441**	0.405**	0.342**	0.215*	-0.043	-0.394**	-0.614**	-0.700**	-0.681**
MFD	-0.044	-0.054	-0.068	-0.085	-0.114	-0.161	-0.210*	-0.247*	-0.329**	-0.619**
Annual										
AT	0.932**	0.932**	0.931**	0.927**	0.917**	0.899**	0.862**	0.794**	0.700**	0.612**
TPR	0.366*	0.371*	0.379*	0.388*	0.400*	0.414*	0.431*	0.447*	0.456**	0.454**
MSD	-0.353*	-0.357*	-0.362*	-0.368*	-0.375*	-0.385*	-0.397*	-0.406*	-0.407*	-0.397*
MFD	-0.631**	-0.638**	-0.653**	-0.677**	-0.709**	-0.756**	-0.818**	-0.890**	-0.949**	-0.981**

251 In the four seasons, the TPR and the ST are also significantly correlated, with all
 252 the Rs passing the 0.01 significance test except that at 21.2 cm and 36.6 cm in winter.
 253 In winter and spring, the precipitation on the TP is mainly from snow, which covers
 254 the ground to hinder the land-air interaction and reduce the soil heat loss, resulting in
 255 higher ST in shallow layers (Bian et al. 2017; Fu et al. 2018; Luo et al. 2020).
 256 However, the snow cover in winter favors the transport of soil heat flux from deep to
 257 shallow layers, making the deep soil temperature lower (Wang et al. 2019), so the
 258 TPR is negatively correlated with the ST. In summer and autumn, the liquid
 259 precipitation can increase the soil water content, thus increasing the heat capacity of
 260 the soil (Qian et al. 2010; Zhang et al. 2004), therefore, the TPR is generally
 261 positively correlated with the ST. The influence of the total precipitation on the ST is
 262 strongest in autumn with an average R of 0.836, followed by spring (average R of
 263 0.824), summer (average R of 0.575), and winter (average Rs of 0.301 and -0.413 in
 264 the shallow-middle layers and the deep layer, respectively). The effect of precipitation
 265 on the ST is quite complex. The Rs increase gradually with soil depth in the
 266 0.7~103.8 cm layers in spring and the 0.7~11.9 cm layers in summer. In autumn, the
 267 Rs decrease with soil depth through the entire soil column, and the annual mean Rs

increase with soil depth, with the significance increasing as well. It is mainly attributed to the freeze-thaw process of the soil, in which the freezing of the soil prevents the infiltration of liquid water (Gao et al. 2018; Guo et al. 2011).

The inhibitory effect of snow cover on the land-air heat exchange depends on the timing, duration, accumulation, and melting processes of snow cover (Zhang 2005; Wang 2017). In spring, the R between the ST and the MSD fails the 0.05 significance test. In winter, the snow cover significantly increases the ST in the shallow and middle layers (average R of 0.374) but decreases the ST in the deep layers (average R of -0.486). This confirms that the snow cover can promote the soil heat flux transport from the deep to the shallow layers. In summer and autumn, the snow cover mainly remains near the Kunlun Mountains in the western TP, which restrains the ST increase, with R_s of -0.772 and -0.743, respectively. The absolute values of the R_s increase with soil depth in summer (0.7~103.8 cm soil layers) and autumn (0.7~6.2 cm soil layers). For the annual average, the snow cover also inhibits soil warming, and the absolute values of the R_s between the MSD and the ST increase with soil depth in the 0.7~172.8 cm layers.

The MFD is negatively correlated with the ST, and the annual average R_s pass the 0.01 significance test in all the layers. In addition, the absolute value of the R_s increases with soil depth, reaching -0.981 at the 286.5 cm layer. However, the R_s between the ST and the MFD fail the 0.05 significance test in the 0.7~36.6 cm layers in spring and winter and in the 0.7~103.8 cm layers in autumn. In summer, the R_s pass the 0.01 significance test in all the layers. The absolute values of the R_s are the largest among the four seasons, which increase with soil depth in the 2.8~21.2 cm layers and 62.0~286.5 cm layers. It can be revealed that the MFD has the strongest inhibitory effect on the soil warming in summer, and the effect strength increases with soil depth.

In summary, the AT, the TPR, the MSD and the MFD are all significantly correlated with the ST, with the influence degree of AT, MFD, TPR and MSD in descending order. In addition, the influence degree varies significantly with season and soil layer. The AT and the TPR promote soil warming, while the MSD and the MFD inhibit it. The contribution of AT is significant in all seasons and decreases with the increasing soil depth. The contribution of TPR to the ST is more complex, with the strongest effect in autumn, and the effect intensity mainly increases with the increasing soil depth. The MSD inhibits the soil warming mainly in summer and autumn, while winter snow cover has an insulating effect on the shallow and the middle soil layers. The inhibitory effect of MFD on the soil warming is mainly observed in summer, and the effect intensity increases with soil depth.

4. Summary and discussion

A coupled regional climate model was utilized to simulate the land surface processes on the TP for 32 years. The monthly ST variation, the climatic trend of the ST on annual, seasonal and monthly scales and the correlations between the ST variation and the AT, the TPR, the MSD and the MFD are analyzed. The main conclusions are as follows.

The ST has an evident interannual variation. Since temperature transfer in the soil requires a certain time, the monthly variation of deep soil temperature lags slightly behind that in the shallow and middle layers. The STs in 0.7~286.5 cm layers increase from 1987 to 2018, and the warming trends are slightly higher in October-May ($0.040\text{ }^{\circ}\text{C}\cdot\text{decade}^{-1}$) than in June-September ($0.026\text{ }^{\circ}\text{C}\cdot\text{decade}^{-1}$), with the maximum warming trend occurring in February ($0.058\text{ }^{\circ}\text{C}\cdot\text{decade}^{-1}$). In terms of spatial distribution, the warming is more significant in the TRSR ($0.15\sim0.20\text{ }^{\circ}\text{C}\cdot\text{decade}^{-1}$) located in the southeast part of the TP and near the Himalayas and the Kunlun Mountains ($0.20\sim0.25\text{ }^{\circ}\text{C}\cdot\text{decade}^{-1}$). In addition, the warming trends in winter and spring are higher than those in summer and autumn. The soil warming trend decreases with the increase of soil depth, while the sign of the trend keeps consistent.

The AT, the TPR, the MSD, the MFD can all significantly affect the ST. The AT and the TPR can accelerate the soil warming, while the MSD and the MFD can slow down it. The influence of AT on the ST warming is intense in all seasons ($R\geq0.85$), while it is greater in spring ($R=0.928$) than in autumn ($R=0.892$), summer ($R=0.957$) and winter ($R=0.560$), and the influence intensity decreases with the increasing soil depth. The effect of TPR on the ST is relatively complex because the freeze-thaw process of the soil prevents the infiltration of liquid water, and its main effect occurs in autumn ($R=0.836$). The snow cover in winter causes the shallow and middle STs to increase and deep STs to decrease. The residual snow cover in summer slows down the soil warming trend, and the effect of MSD on the ST increases with the increasing soil depth. Except for AT, the change in MFD in summer has the greatest effect on the ST ($R=-0.77$), and the effect intensity increases with the increasing soil depth.

By using the numerical model, this paper systematically explores the ST trends on the TP from 1987 to 2018, with the warming trend of FG on the TP and the influences of multiple factors on it further verified. It makes up for the lack of observational data on the western TP, however, the investigation is still limited. The freeze-thaw process in the permafrost and the SFG are quite different. The SFG completely melts in summer, while the deep soil in the permafrost regions remains frozen. This makes their responses to climate change potentially different. More scientific conclusions can be achieved by accurately determining the distribution of different FG on the TP and then analyzing the effects of AT, TPR, MSD, MFD, etc. on FG specifically.

The FG warming trend varies with altitudes (Li et al. 2012, Gao et al. 2018). The annual average soil warming is slightly weaker at higher altitudes in the western part of TP than in the southern and east-central parts (Figure 3~5). It has also been pointed out that the freeze-thaw process of FG causes energy imbalance (Guo et al. 2011), and the rapid warming on the TP also enhances radiative cooling and surface evaporation (Yang et al. 2014). Thus, change in the radiative transfer is also an important exogenous factor of FG changes on the TP. Both numerical experiments (Cuo et al. 2015, Gao et al. 2018, Guo and Wang 2013) and observational data analyses (Luo and Wang 2020, Wang et al. 2020) have shown that the FG on the TP is in an obvious degradation process. Therefore, it's the consequent hydrological, ecological, and

climatic effects deserve sufficient attention. Further simulation validation can be done using multiple numerical models in future work, which can also provide a scientific basis for the improvement of the freeze-thaw parameterization scheme.

Acknowledgements. This research was jointly supported by the Second Tibetan Plateau Scientific Expedition and Research (STEP) Project (2019QZKK0103), the National Natural Science Foundation of China (Grants 41775016, 41975007, and 41905008), and the Scientific Research Foundation of CUIT (KYTZ201822). We thank Nanjing Hurricane Translation for reviewing the English language quality of this paper.

References

- Beheng KD (1994) A parameterization of warm cloud microphysical convection process. *Atmos. Res.*, 33: 193-206.
- Bian QY, Lyu SH, Wen LJ, Li ZG, Chen SQ (2017) Soil Freezing-thawing Process and Its Temperature and Moisture Conditions in High and Low Snowfall Years in Headwaters of the Yellow River. *Arid Zone Research*, 34(4): 906-911.
- Chen J, Sheng Y, Cheng GD (2006) Discussion on Protection Measures of Permafrost under the Action of Engineering from the Point of Earth Surface Energy Balance Equation in Qinghai-Tibetan Plateau. *Journal of Glaciology and Geocryology*, 28(2): 223-228.
- Cuo L, Zhang YX, Bohn TJ, Zhao L, Li JL, Liu QM, Zhou BR (2015) Frozen soil degradation and its effects on surface hydrology in the northern Tibetan Plateau. *J. Geophys. Res. Atmos.*, 120(16): 8276-8298.
- Emanuel KA (1991) A scheme for representing cumulus convection in large-scale models. *J. Atmos. Sci.*, 48: 2313-2335.
- Fang XW, Luo SQ, Lyu SH (2019) Observed soil temperature trends associated with climate change in the Tibetan Plateau, 1960–2014. *Theoretical and Applied Climatology*, 135: 169–181. <https://doi.org/10.1007/s00704-017-2337-9>.
- Fang YP, Zhu FB, Yi SH, Qiu XP, Ding YJ (2019) Contribution of permafrost to grassland ecological carrying capacity in the Qinghai-Tibetan Plateau. *Climate Change Research*, 15(2): 150-157.
- Fu Q, Hou RJ, Li TX, Jiang RQ, Yan PR, Ma Z, Zhou ZQ (2018) Effects of soil water and heat relationship under various snow cover during freezing-thawing periods in Songnen Plain, China. *Scientific Reports*, 8(1): 1-12.
- Gao B, Yang DW, Qin Y, Wang YH, Li HY, Zhang YL, Zhang TJ (2018) Change in frozen soils and its effect on regional hydrology, upper Heihe basin, northeastern Qinghai-Tibetan Plateau. *Cryosphere*, 12(8):657-673.
- Gao JQ (2017) Frozen ground response to climate change and the POD-based reduced-order extrapolating model. Beijing, China: North China Electric Power University.
- Gao X, Shi Y, Song R, Giorgi F, Wang Y, Zhang D (2008) Reduction of future monsoon precipitation over China: Comparison between a high-resolution RCM simulation and the driving GCM. *Meteorology and Atmospheric Physics*, 100: 73-86.
- Giorgi F (1990) Simulation of regional climate using a limited area model nested in a general circulation model. *J. Climate*, 3: 941-963.
- Guo DL, Yang MX, Wang HJ (2011) Characteristics of land surface heat and water exchange under different soil freeze/thaw conditions over the central Tibetan Plateau. *Hydrological Processes*, 25(16): 2531-2541.

- Guo DL, Wang HJ (2013) Simulation of permafrost and seasonally frozen ground conditions on the Tibetan Plateau, 1981–2010. *Journal of Geophysical Research: Atmospheres*, 118(11): 5216-5230.
- Hamed KH, Rao AR (1998) A modified Mann-Kendall trend test for autocorrelated data. *J Hydrol*, 204: 182-196.
- Holtzlag AAM, de Bruijn EIF, Pan HL (1990) A high-resolution air mass transformation model for short-range weather forecasting. *Mon. Wea. Rev.*, 118: 1561-1575.
- Kendall MG (1955) Rank correlation methods. Charles Griffin & Co, London.
- Kong X H, Wang A H, Bi X Q, Wang D (2019) Assessment of temperature extremes in China using RegCM4 and WRF. *Advances in Atmospheric Sciences*, 36(4): 363-377.
- Li SY, Yang K, Wang CH (2018) Bias characteristics of the land surface model (CLM4.5) over the Tibetan Plateau during soil freezing-thawing period and its causes. *Journal of Glaciology and Geocryology*, 2018, 40(2): 322-334.
- Li X, Jin R, Pan XD, Zhang TJ, Guo JW (2012) Changes in the near-surface soil freeze-thaw cycle on the Qinghai-Tibetan Plateau. *International Journal of Applied Earth Observations & Geoinformation*, 17(1): 33-42.
- Li XL (2013) Study on the relationship between the temporal & spatial of snow cover in winter and spring over Tibetan Plateau and the summer precipitation in Eastern China. Lanzhou, Gansu, China: Lanzhou University.
- Luo JX, Lyu SH, Ma CL, Fang XW (2020) Simulation analysis of soil water and heat characteristics in high and low snowfall years on the Qinghai-Tibetan Plateau. *Plateau Meteorology*, 39(6): 1-12. DOI:10.7522/j.issn.1000-0534.2020.00031.
- Luo SQ, Fang XW, Lyu SH, Ma D, Chang Y, Song MH, Chen H (2016) Frozen ground temperature trends associated with climate change in the Tibetan Plateau Three River Source Region from 1980 to 2014. *Climate Research*, 67(3): 241-255.
- Luo SQ, Wang JY, Pomeroy JW, Lyu SH (2020) Freeze-Thaw Changes of Seasonally Frozen Ground on the Tibetan Plateau from 1960 to 2014. *Journal of Climate*, 33: 9427-9446.
- Mackay A (2008). *Climate Change 2007 : Impacts, adaptation, and vulnerability. Contribution of working group II to the fourth assessment report of the intergovernmental panel on climate change.* *Journal of Environmental Quality*, 37(6): 2407.
- Mann HB (1945) Nonparametric tests against trend. *Econometrica*, 13: 245-259.
- Qian YF, Zheng YQ, Zhang Y, Miao MQ (2010) Responses of China's summer monsoon climate to snow anomaly over the Tibetan Plateau. *International Journal of Climatology*, 23(6): 593-613.
- Sen PK (1968) Estimates of the regression coefficient based on Kendall's Tau. *J Am Stat Assoc*, 63: 1379-1389.
- Wang CH, Dong WJ, Wei ZG (2001) The feature of seasonally frozen soil in Qinghai-Tibet Plateau. *Acta Geographica Sinica*, 56(5): 523-531.
- Wang CH, Dong WJ, Wei ZG (2003) Study on the relationship between the frozen-thaw process in Qinghai-Xizang Plateau and circulation in East-Asia. *Chinese Journal of Geophysics*, 46(3): 309-316.
- Wang CH, Zhao W, Cui Y (2020) Changes in the Seasonally Frozen Ground Over the Eastern Qinghai-Tibet Plateau in the Past 60 Years. *Frontiers in Earth Science*, 8:270.
- Wang R, Zhu QK, Ma H, Ai N (2017) Spatial-temporal variations in near-surface soil freeze-thaw cycles in the source region of the Yellow River during the period 2002–2011 based on the Advanced Microwave Scanning Radiometer for the Earth Observing System (AMSR-E) data. *Journal of Arid Land*, 9(6): 850–864.
- Wang SJ (2017) Progresses in the variability of snow cover over the Qinghai-Tibetan Plateau and its impact on water resources in China. *Plateau Meteorology*, 36(5): 1153-1164. DOI:10.7522/j.issn.1000-0534.2016.00117.
- Wang T, Li ZG, Lyu SH (2019) Study on the effects of snow cover on heat transport in the land surface process

441 over Qinghai-Tibetan Plateau. Plateau Meteorology, 38(5): 920-924.
 442 DOI:10.7522/j.issn.1000-0534.2019.00026.
 443 Wu QB, Zhang TJ (2010) Changes in active layer thickness over the Qinghai-Tibetan Plateau from 1995 to 2007.
 444 Journal of Geophysical Research: Atmospheres, 115(9): 1-12.
 445 Xie ZP, Hu ZY, Liu HL, Sun GH, Yang YX, Lin J, Huang FF (2017) Evaluation of the surface energy exchange
 446 simulations of land surface model CLM4.5 in the alpine meadow over the Qinghai-Xizang Plateau. Plateau
 447 Meteorology, 36(1): 1-12. DOI: 10.7522/j.issn.1000-0534.2016.00012.
 448 Yang K, Wu H, Qin J, Lin CG, Tang WJ, Chen YY (2014) Recent climate changes over the Tibetan Plateau and
 449 their impacts on energy and water cycle: A review. Global and Planetary Change, 112(1):79-91.
 450 Yu L (2011) Simulation study on the characteristics of climate change and over Tibet Plateau. Lanzhou, Gansu,
 451 China: Lanzhou University.
 452 Zeng X, Zhao M, Dickinson RE (1998) Intercomparison of bulk aerodynamic algorithms for the computation of
 453 sea surface fluxes using TOGA COARE and TAO data. J. Climate, 11:2628-2644.
 454 Zhang T J (2005) Influence of the seasonal snow cover on the ground thermal regime: An overview. Reviews of
 455 Geophysics, 43(4): RG4002.
 456 Zhang YS, Li T, Wang B (2004) Decadal Change of the Spring Snow Depth over the Tibetan Plateau: The
 457 Associated Circulation and Influence on the East Asian Summer Monsoon. Journal of Climate, 17(14):
 458 2780-2793.
 459 Zhao HX, Moore GWK (2004) On the relationship between Tibetan snow cover, the Tibetan plateau monsoon and
 460 the Indian summer monsoon. Geophysical Research Letters, 31(14): 101-111.
 461 Zhou JW (2007) Simulation of the effect of anomalous Plateau snow cover and SSTA on summer climate of
 462 northwest China. Nanjing, Jiangsu, China: Nanjing University of Information Science & Technology.
 463 Zhou YW, Guo DX (1982) Principal characteristics of permafrost in China. Journal of Glaciology and
 464 Geocryology, 4(1): 1-12.